Journal of Nuclear Materials 508 (2018) 319–328

Contents lists available at ScienceDirect

Journal of Nuclear Materials

journal homepage: www.elsevier.com/locate/jnucmat

Vaporization behaviour of the Molten Salt Fast Reactor fuel: The LiF-ThF_4-UF_4 system

A. Tosolin [a, b], O. Beneš [a, *], J.-Y. Colle [a], P. Souček [a], L. Luzzi [b], R.J.M. Konings [a]

[a] European Commission, Joint Research Centre, P.O. Box 2340, 76125, Karlsruhe, Germany
[b] Politecnico di Milano, Department of Energy, Via La Masa 34, 20156, Milan, Italy

HIGHLIGHTS

- First experimental results for a selected mixture for the European Molten Salt Fast Reactor.
- Boiling point determined by extrapolation of experimental results.
- Results compared with calculated values and ideal behaviour.
- Novel measurements for the vapour pressure of pure UF_4.

ARTICLE INFO

Article history:
Received 6 March 2018
Received in revised form
3 May 2018
Accepted 22 May 2018
Available online 23 May 2018

Keywords:
Molten Salt Reactor
Knudsen effusion mass spectrometry
Vapour pressure
Actinide fluorides
Thermodynamic activities

ABSTRACT

A selected composition of the initial fuel of the Molten Salt Fast Reactor (MSFR) is assessed by differential scanning calorimetry (DSC) for melting point determination and by Knudsen effusion mass spectrometry (KEMS) for vaporization behaviour. Partial vapour pressures and thermodynamic activities of the MSFR fuel mixture are discussed indicating departures from ideal behaviour, and further interpreted by phase equilibria calculations. The boiling point of the mixture is obtained extrapolating vapour pressure experimental results. New results on the vaporization behaviour of pure uranium tetrafluoride are presented, together with the ionization potentials of UF_4 by electron impact.

1. Introduction

Molten Salt Reactors (MSRs) are a family of fission reactors in which the thermal carrier is a liquid mixture of inorganic salts. One of the important features of the concept is that the nuclear fuel can be dissolved in the coolant providing a homogenous core with the possibility of a continuous online fuel reprocessing [1]. At the beginning of the new millennium, the Generation IV International Forum (GIF) selected the MSR among the six most promising future reactors [2], especially because of its potentials in safety, sustainability, economics and non-proliferation [3]. The interest for this technology grew and spread in several countries, involving also private investors. A consortium of European Union (EU) member state organisations is particularly interested and since 2001 has been working for the development of a large size MSR able to fulfil the ambitious goals set by GIF. Since then, the studies have focussed on a thorium-fuelled non-moderated version because the use of thorium can bring significant advantages: it is more abundant in earth crust than uranium, and can be used to sustain a $^{232}Th/^{233}U$ fuel cycle in a breeding mode [4]. This concept, called Molten Salt Fast Reactor (MSFR) [5], is currently under consideration by GIF [6] and studied within the European Horizon2020 project SAMOFAR [7], which has the main objective of evaluating the innovative safety features of the MSFR.

The reference MSFR has a power output of 3000 MW_{th} with a total fuel salt volume of 18 m^3 and a fertile blanket around the core to increase the breeding gain [8]. The initial fuel composition is a binary mixture composed of 77.5 mol% of lithium fluoride and 22.5 mol% of heavy nuclei (HN) in form of fluorides. Lithium is enriched in ^7Li to 99.995 at% for reducing neutron parasitic absorptions. The exact amount of ThF_4, UF_4 and other actinide

* Corresponding author.
E-mail address: Ondrej.BENES@ec.europa.eu (O. Beneš).

https://doi.org/10.1016/j.jnucmat.2018.05.049

fluorides depends on the particular application (breeder, incinerator, etc.) and the availability of fissile material, which could be [9]:

- uranium-233 obtained from thorium-232 in other breeder reactors;
- enriched uranium with an enrichment ratio lower than 20% due to nuclear proliferation resistance;
- plutonium-239 and minor actinides produced in commercial nuclear reactors currently under operation;
- a mix of the solutions above.

In this study, we focus on a fuel composition based on Th/U fuel cycle. In this case, the design parameters require an amount of uranium tetrafluoride of 2.5 mol% [10], so that the reference initial composition of the MSFR started with uranium-233 is LiF-ThF_4-UF_4 (77.5-20.0-2.5 mol%), identified in SAMOFAR project.

The thermo-physical and thermo-chemical properties of this mixture must be studied in detail for assessing the safety features of the MSFR and for the optimization of many reactor operation parameters in view of the strong coupling between physical, chemical and hydraulic characteristics of the circulating liquid. Within this framework, knowing the properties in the vapour phase in equilibrium with the liquid is crucial for predicting the fuel behaviour in both normal and accidental conditions.

In this paper, a thorough investigation of the vaporization behaviour of the LiF-ThF_4-UF_4 system by Knudsen effusion mass spectrometry (KEMS) is presented, coupling experimental results and thermodynamic modelling. The thermodynamic activities of the end-members are taken into account for pointing out if any departures from ideal behaviour. Results for the LiF and ThF_4 end members are taken from our previous work [11], while new results on the vaporization of pure UF_4 are presented.

2. Experimental

2.1. Initial materials

The mixture assessed in this study is LiF-ThF_4-UF_4 (77.5-20.0-2.5 mol%). Lithium fluoride was purchased from Alfa Aesar, which declares metal-base purity of 99.99%. Thorium and uranium tetrafluorides were synthetized by hydrofluorination. For details about the synthesis of these actinide fluorides we refer to our previous work [12]. Because fluorides are hygroscopic, all initial materials were stored and handled inside an argon glove box, in which the concentration of oxygen and moisture is continuously monitored and kept below 2 ppm. Before use, LiF was purified in a process which consists in heating up to 400 °C in argon flow for 4 h, long enough to vaporize the contained moisture. The final mixture (of about 500 mg batch) was prepared by mixing the end-members in an agate mortar.

2.2. Differential scanning calorimetry

Phase equilibria temperatures of condensed phases were measured by differential scanning calorimetry (DSC). The technique allows to evaluate the purity of the materials through the measurement of the melting point of the end-members, which in absence of impurities should appear as clear single peak, reproducing the correct temperature (if known). The apparatus used in this work is a Setaram Multi-detector High Temperature Calorimeter (MHTC 96) equipped with a DSC sensor with S-type thermocouples.

Because fluoride vapours can become corrosive at high temperature and can damage the interior of the device, the samples were encapsulated in stainless steel crucibles with an internal nickel liner for chemical compatibility [13]. For more details about the encapsulation technique we refer to our previous work [14]. The temperature measured by the device is corrected by a calibration curve based on a series of experiments for the melting point determination of reference materials (Sn, Pb, Zn, Al, Ag, Cu).

The DSC experiments consisted in two consecutive heating ramps at 10 K/min from room temperature up to 1200 °C, well above the melting point of the highest melting end-member. The first ramp was for reaching a better mixing and a homogenous sample. The melting points reported in this work refer to the second ramp. To verify the results obtained at 10 K/min, we additionally performed experiments at 5 K/min and obtained consistent results (Section 3.1).

2.3. Knudsen effusion mass spectrometry

Thermodynamic properties of gaseous phase were measured by Knudsen effusion mass spectrometry (KEMS) [15,16]. The device consists of a Knudsen cell heated by a tungsten coil and coupled with a quadrupole mass spectrometer. The facility [17] is specifically designed for radioactive materials and it has been successfully used for different applications [18]. The Knudsen cell is made of tungsten and the dimensions are summarized in Table 1.

Before the measurement, the experimental chamber was evacuated to high vacuum (10^{-6} mbar) for avoiding interactions between the sample and the atmosphere. The experiment consisted in a heating ramp at 10 K/min, continuing up to the complete vaporization of the sample. The molecules escaping from the cell orifice are subjected to an electron beam which ionizes some of them. The electron beam may also produce fragmentation of molecules in smaller ions. An electric field separates the ionized molecules according to their masses, allowing their detection by the mass spectrometer, which gives a signal proportional to the partial vapour pressure. Because of the fragmentation in smaller ions, the signal coming from one species must be constructed taking into account the different contributions. The temperature inside the cell is measured by a pyrometer calibrated using the melting point of standard materials (Zn, Cu, Fe, Pt, and Al_2O_3). The average energy value of the electron beam was calibrated using the ionization potential of different pure elements (Ar, Kr, Xe, Zn, In and Ag). During the experiment, the intensity of the electron beam was kept constant at 32.85 eV. The only exception was a period of 15 min during which the temperature was kept constant and the electron energy was gradually increased at a constant rate of about 3 eV/min, from 2.8 eV up to 45.1 eV. This procedure allows measuring the minimum energy required to create ions (directly or following fragmentation) by electron impact [19]. In this way it is also possible distinguishing the species produced by fragmentation from those with the same mass, released in form of vapour by the sample in the Knudsen cell. It is important to perform this measurement when the vaporization of the sample is significant.

In the simplest case (no fragmentation following electron impact and only monoisotopic species in the vapour), the partial vapour pressure of a species *i*, at the temperature *T* can be written as

Table 1
Characteristic dimensions of the Knudsen cell used in this work.

Dimension	Value [mm]
Cell diameter	11
Cell height	21
Orifice diameter	0.5
Orifice edge thickness	0.25

$$p_i = K_i \cdot T \cdot I_i^+ \quad (1)$$

in which T is the temperature detected by the pyrometer, I_i^+ is the signal of the mass spectrometer and K_i is a coefficient of proportionality. K_i depends on many factors, among which:

- the geometry of the Knudsen cell;
- the path travelled by the species from the Knudsen cell up to the mass spectrometer;
- the efficiencies of the various devices as the mass spectrometer and the electron beam generator;
- the molar mass of the species i;
- the cross section of the ionization reaction

$$i + e^- \rightarrow i^+ + 2e^- \quad (2)$$

In this work, K_i is determined by putting a few mg of silver as calibration material in the Knudsen cell together with the sample. Since the vapour pressure of silver is well known [20], all the geometrical and instrumental contribution to K_i are taken into account measuring the signals of the two isotopes of silver ($I_{Ag}^+ = I_{107Ag}^+ + I_{109Ag}^+$):

$$K_{Ag} = \frac{p_{Ag}}{I_{Ag}^+ \cdot T} \quad (3)$$

As far as Knudsen flow conditions are respected (Knudsen number $Kn > 0.01$) [21], we can assume that the flow of the vapour molecules through the orifice does not affect the equilibrium inside the Knudsen cell, so that K_{Ag} is a constant. In several experiments carried out we observed that above a few tens of pascal, the mass spectrometer signal of silver has a different trend from the vapour pressure of silver reported in literature, indicating departure from Knudsen conditions and setting the upper limit for the measurement performed in this study on pure UF_4. For the mixture LiF-ThF_4-UF_4 (77.5-20.0-2.5 mol%) this limit was even lower since we observed above 1200 K total pressure of few pascal. The lower limit is set by several parameters like the sensitivity of the mass spectrometer, the ionization properties of the gaseous species inside the Knudsen cell and possible background in the signal.

The contributions to K_i due to the different masses of the detected species (which affects the gain of the secondary electron multiplier (SEM) of the mass spectrometer [22]) and to the probability that the species are ionized by electron impact, are related to the molar mass and ionization cross section of silver:

$$K_i = K_{Ag} \frac{\sqrt{M_i}}{\sqrt{M_{Ag}}} \frac{\sigma_{Ag}}{\sigma_i} \quad (4)$$

In practical cases, fragmentation by electron impact of the species escaping from the orifice always occurs. The signal of the mass spectrometer must be carefully interpreted for taking into account all the contributions coming from the same species. Since lithium and uranium have more than one isotope, the resulting vapour pressures are accounted for this phenomenon accordingly.

For the determination of the ionization cross sections by electron impact we used for single atoms (e.g., for Ag) the cross sections calculated by Sigma software [23], which bases the computations on the values published by Mann [24]. For the determination of the ionization cross sections of the AB_n-type molecules, we applied the modified additivity role proposed by Deutsch et al [25].:

$$\sigma(AB_n) = \left[\frac{r_A^2}{r_B^2}\right]^{\alpha} \left[\frac{\xi_A}{\xi_A + n\xi_B}\right] \sigma_A + \left[\frac{nr_B^2}{r_A^2}\right]^{\beta} \left[\frac{n\xi_B}{\xi_A + n\xi_B}\right] n\sigma_B \quad (5)$$

in which r_A, r_B and ξ_A, ξ_B refer to the atomic radii and the effective number of electrons of the constituent atoms A and B, respectively. Their values are taken from the tables of Desclaux [26]. The exponents α and β explicitly depend on r_A, r_B and ξ_A, ξ_B, and the procedure for their determination is described in the original paper [25].

The ionization cross section of UF_4 was calculated according to equation (5). Cross-section data and other parameters for LiF and ThF_4 were discussed in our previous work [11]. Since lithium fluoride evaporates also in form of dimer and trimer, which are not of the AB_n-type molecule, we used for these species the cross section values proposed by Yamawaki et al. [27], who performed KEMS measurements with ionizing electron energies fixed to a value of 30 eV, close to the one used in this work. The absolute ionization cross sections of LiF, Li_2F_2 and Li_3F_3 reported in Table 2, come from the ionization cross sections normalized to silver σ_i/σ_{Ag} proposed by Yamawaki et al. [27], considering the ionization cross section of silver used in this work.

The evaporation of LiF is particularly difficult to study by KEMS because it involves different species (monomer, dimer and trimer) which at 32.85 eV produce many different ions by fragmentation. Many authors addressed the topic [27–29] leading to sometimes different conclusions. In this work, we refer to the parameters suggested by Yamawaki et al. [27], who identified Li^+, LiF^+, Li_2F^+ and $Li_3F_2^+$ as the 4 main ions produced by the electron beam. They concluded that Li^+ and LiF^+ are formed by the monomer, Li_2F^+ by the dimer and $Li_3F_2^+$ by the trimer, and attributed normalized SEM gains γ_i/γ_{Ag} (average number of electrons generated by an ion i over the average number of electrons generated by a silver ion), rather different from the normalized square of the molar masses (this equivalence is more reliable for heavy molecules). Equation (4) can then be written as:

$$K_i = K_{Ag} \frac{\gamma_i}{\gamma_{Ag}} \frac{\sigma_{Ag}}{\sigma_i} \quad (6)$$

As suggested by Yamawaki et al. [27], the normalized SEM gains for Li^+, LiF^+, Li_2F^+ and $Li_3F_2^+$ are 0.87, 1.47, 1.66 and 2.48, respectively. This approach is used also in this work for measuring the partial vapour pressure of LiF in the LiF-ThF_4-UF_4 (77.5-20.0-2.5 mol %) system.

For ThF_4 and UF_4 no evidence of associated molecules in the vapour phase was found in this study, confirmed by previous studies too [30]. Nevertheless, at 32.85 eV fragmentation by electron impact of these molecules occurred. The mass spectrometer detected ions with masses corresponding to ThF_3^+, ThF_2^+ ThF^+ and Th^+ from ThF_4, and UF_3^+, UF_2^+ UF^+ and U^+ from UF_4. An appreciable signal indicating the presence of UF_4^+ was also observed (see Fig. 4), but the ion ThF_4^+ was not detected.

Table 2
Cross section values used in this work.

Species i	σ_i [10^{-16} cm^2]	Reference
Ag	5.0458	[23]
LiF	3.0779	[27]
Li_2F_2	3.5825	[27]
Li_3F_3	4.2889	[27]
ThF_4	8.9184	[11]
UF_4	8.8879	This work

3. Results and discussion

The melting point of the mixture LiF-ThF_4-UF_4 (77.5-20.0-2.5 mol%) and of all its end-members was measured in this work. Our results on vapour pressure of UF_4 obtained by KEMS are presented and compared with experimental data of other authors. Activities and experimental results on partial vapour pressures of the MSFR fuel mixture LiF-ThF_4-UF_4 (77.5-20.0-2.5 mol%) are also presented and discussed in this section.

3.1. Melting point

DSC signals of the mixture LiF-ThF_4-UF_4 (77.5-20.0-2.5 mol%) and of the end-members used in this work are shown in Fig. 1.

The obtained melting points are summarized in Table 3. The results for pure components are in good agreement with the experimental data collected by Konings et al. [31], who recommended for LiF the value reported in the NIST-JANAF tables [32], and for ThF_4 a melting point of 1383 ± 3 K, which is in very good agreement with the value measured by several authors [33–36]. For UF_4 previous studies [37,38] suggested a melting point significantly lower than the one recommended in Table 3. For this reason, the melting point of UF_4 was recently determined on a high purity sample in our previous work [12].

The thermodynamic database previously assessed by Capelli et al. [39] was used for calculating the pseudo-binary LiF-ThF_4 phase diagram with 2.5 mol% fixed amount of UF_4, shown in Fig. 2.

As explained in the paper, the database was developed based on thermodynamic assessments of the three binary sub-systems for which equilibrium data existed, and optimization of the unknown thermodynamic parameters, which in this case are the Gibbs energy equation of the intermediate compounds and the excess Gibbs parameters of the present solid and liquid solutions. For solid solutions the 2-sublattice model was used, while for the description of the liquid phase the modified quasi-chemical model proposed by Pelton et al. [40] was employed. The Gibbs energy functions of the solution phases of the higher order systems were extrapolated based on the Kohler-Toop mathematical formalism and (where appropriate) optimized with small ternary parameters. For more details about the thermodynamic modelling we refer to our earlier cited study [39].

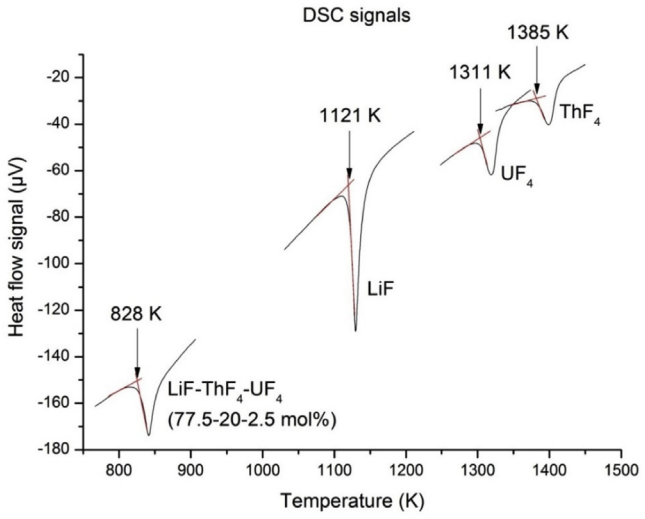

Fig. 1. DSC signals for the LiF-ThF_4-UF_4 (77.5-20.0-2.5 mol%) mixture and its end-members.

Table 3
Melting points measured by DSC.

Sample	T_{melt} [K]	Recommended [K]
LiF	1121 ± 3	1121 ± 1 [32]
ThF_4	1385 ± 3	1383 ± 3 [31]
UF_4	1311 ± 3	1309 ± 3 [12]
LiF-ThF_4-UF_4 (77.5-20.0-2.5 mol%)	828 ± 3	–

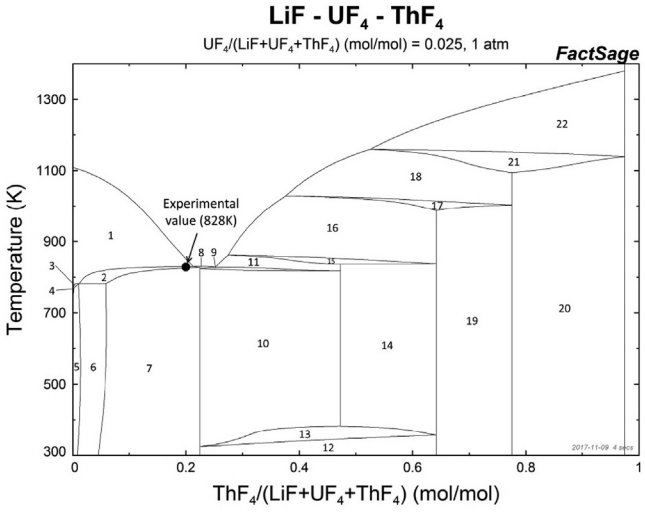

Fig. 2. Pseudo-binary LiF-ThF_4 phase diagram with 2.5 mol% of UF_4. Phase fields: (1) liquid + LiF; (2) liquid + LiF + $Li_3(Th,U)F_7$; (3) $Li3(Th,U)_6F_{31}$ + LiF; (4) $Li_7(Th,U)_6F_{31}$ + Li_4UF_8 + LiF; (5) $Li_3(Th,U)_6F_{31}$ + LiF; (6) $Li_3(Th,U)F_7$ + $Li_7(Th,U)_6F_{31}$ + LiF; (7) $Li_3Th,U)F_7$ + LiF; (8) $Li_3Th,U)F_7$ + liquid; (9) $Li_3(Th,U)F_7$ + $Li_7(Th,U)_6F_{31}$ + liquid; (10) $Li_3(Th,U)F_7$ + $Li_7(Th,U)_6F_{31}$; (11) $Li_7(Th,U)_6F_{31}$ + liquid; (12) $Li(Th,U)_2F_9$ + $Li_3(Th,U)F_7$; (13) $Li(Th,U)_2F_9$ + $Li_3(Th,U)F_7$ + $Li_7(Th,U)_6F_{31}$; (14) $Li(Th,U)_2F_9$ + $Li_7(Th,U)_6F_{31}$; (15) $Li(Th,U)_2F_9$ + $Li_7(Th,U)_6F_{31}$ + liquid; (16) $Li(Th,U)_2F_9$ + liquid; (17) $Li(Th,U)_2F_9$ + $Li(Th,U)_4F_{17}$ + liquid; (18) $Li(Th,U)_4F_{17}$ + liquid; (19) $Li(Th,U)_2F_9$ + $Li(Th,U)_4F_{17}$; (20) $Li(Th,U)_4F_{17}$ + $(Th,U)F_4$; (21) $Li(Th,U)_4F_{17}$ + $(Th,U)F_4$ + liquid; (22) $(Th,U)F_4$ + liquid.

The diagram also shows the experimental melting point temperature measured by DSC (Table 3), which perfectly lies on the line representing the eutectic melting on the phase diagram. It was not possible measuring the liquidus point because (according to the calculated phase diagram) the difference from the corresponding solidus point is smaller than the DSC peak broadness.

3.2. Vapour pressure of uranium tetrafluoride

The vapour pressure of uranium tetrafluoride was measured experimentally by several authors [38,41–47]. In this work, vapour pressure data were collected in the range 1081–1200 K. The melting point was not reached because the complete evaporation of the sample occurred first, due to high vacuum during the experiment.

If the material under investigation does not undergo a phase transformation and evaporates congruently, the logarithm of its vapour pressure versus the reciprocal temperature is well approximated by a linear function. The vapour pressure results of solid UF_4 obtained in this work are listed in Annex Table 1 and are well represented by the following equation:

$$\ln p(Pa) = -\frac{(35758 \pm 357)}{T(K)} + (33.493 \pm 0.216) \quad (7)$$

The lines obtained fitting the experimental data measured by several authors are plotted in Fig. 3.

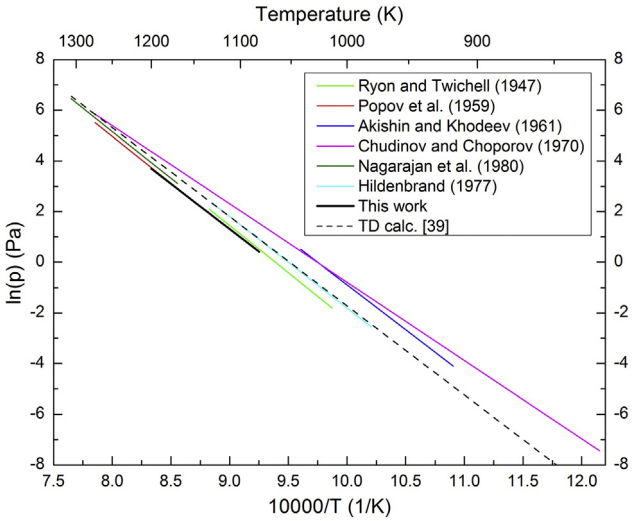

Fig. 3. Vapour pressures for solid UF_4 calculated using experimental data of several authors (solid lines) and the thermodynamic assessment by Capelli et al. [39] (dashed line). Relative uncertainty on UF_4 vapour pressure results obtained in this work is 50%.

Only data on solid UF_4 were considered. The figure also shows (dotted line) the values calculated using the thermodynamic database assessed by Capelli et al. [39]. Despite a slightly different slope, our data are in good agreement with experimental data of Ryon and Twichell [41], Popov et al. [38] and Nagarajan et al. [46].

The errors for slope and intercept in Equation (7) refer to the estimated uncertainty, which in this case depends firstly on the uncertainties on the parameters described in Section 2.3. In this regard, ionization cross sections of molecules by electron impact are rather difficult to determine with high accuracy and precision. As described in Section 2.3, ThF_4 and UF_4 ionization cross sections were calculated according to the modified additivity rule suggested by Deutsch et al. [25], who showed that in most cases their method yields cross sections which agree reasonably with available experimental data, with deviations rarely larger than 20%. Furthermore, also the temperature measurement may represent a source of uncertainty. Despite the calibration (described in Section 2.3), the heating element and the quartz optical window crossed by the laser may affect the temperature registered by the pyrometer. In order to take into account possible deviations from the real temperature, we considered a relative uncertainty on the temperature equals to ±1%. In the light of these considerations (on cross section and temperature), we estimate for our vapour pressure results a confidence interval equals to ±50%.

Enthalpy of sublimation was determined based on vapour pressure results measured in this work according to the second law method:

$$\Delta H^{\circ}_{T_M} = -R\frac{d(\ln K_{eq})}{d(1/T)} \tag{8}$$

and the third law method:

$$\Delta H^{\circ}_{298} = -T\left[R\ln K_{eq} + \Delta\frac{G^{\circ}_T - H^{\circ}_{298}}{T}\right] \tag{9}$$

where T_M is the mean temperature of the measurement, R is the universal gas constant, K_{eq} is the equilibrium constant of the sublimation reaction and $\Delta[(G^{\circ}_T - H^{\circ}_{298})/T]$ is the change of the Gibbs energy function of the reaction considered. In this work, thermodynamic functions of UF_4 are taken from literature [48,49]. The second and third law methods, which are described in detail elsewhere [50], give values of $\Delta H^{\circ}_{298} = 314.0\pm0.8\ kJ/mol$ and $\Delta H^{\circ}_{298} = 314.4\pm0.4\ kJ/mol$, respectively. The indicated errors represent the standard deviation. The value obtained from the third law treatment is more reliable since it does not depend from other vapour pressure results taken at different temperatures. However, the two approaches lead almost to the same value.

Table 4 shows the values calculated by a third law method of the available literature data and shows that our result is in good agreement with the values obtained using the experimental data of Langer and Blankship [42], Hildenbrand [45] and Nagarajan et al. [46].

Finally, the ionization efficiency curves for the ions obtained from UF_4 increasing the electron energy and keeping the temperature constant at 1188 K (high enough to get good signal) are shown in Fig. 4.

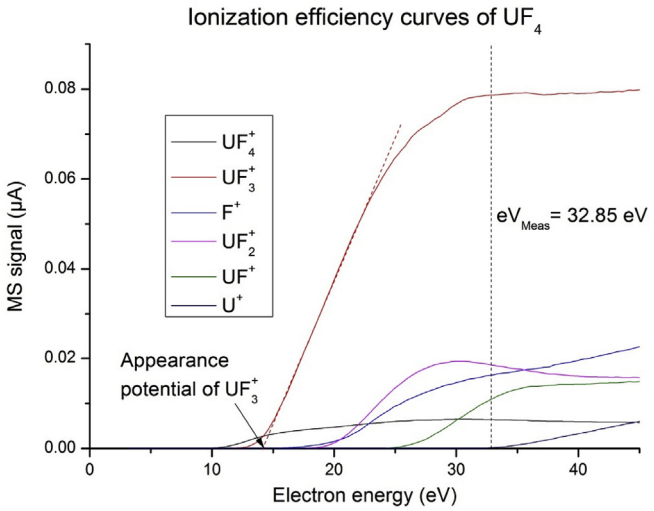

Fig. 4. Ionization efficiency curves measured for the ions F^+, U^+, UF^+, UF_2^+, UF_3^+ and UF_4^+.

Table 4
Enthalpy of sublimation at 298.15 K for UF_4 obtained by third law analysis of experimental data of different authors [48].

Reference	T range [K]	Technique	ΔH°_{298} [kJ/mol]
Popov et al. [38]	1148–1273	Transpiration	318.4 ± 1.0
Langer and Blankenship [42]	1291–1573	Quasistatic and boiling point	313.9 ± 0.2
Akishin and Khodeev [43]	917–1041	Effusion mass spectrometry	344.0 ± 3.0
Chudinov and Choporov [44]	823–1280	Effusion	309.7 ± 0.5
Hildenbrand [45]	980–1130	Torsion-effusion	313.1 ± 0.4
Nagarajan et al. [46]	1169–1427	Transpiration and evaporation	314.5 ± 0.4
Johnsson [47]	1120–1275	Balanced diaphragm method	306.8 ± 0.7
This work	1081–1200	Effusion mass spectrometry	314.4 ± 0.4

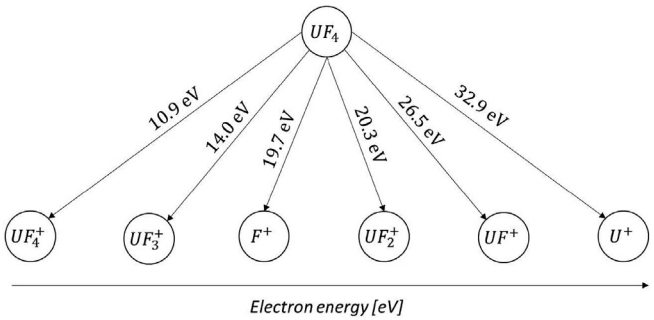

Fig. 5. Appearance potentials of ions from UF_4 molecules by electron impact.

As discussed in Section 2.3, this procedure is needed to correct for the possible fragmentation; but in this case it was simple as all ions detected by the mass spectrometer come from the same species (UF_4(g)). The picture also shows how to get the appearance potential of an ion. Fig. 5 summarizes the ionization potentials obtained in this work for UF_4.

The value of 10.9 eV for the reaction.

$$UF_4 + e \rightarrow UF_4^+ + 2e \tag{10}$$

is in perfect agreement with the value measured by Gorokhov et al. [51]. The ionization potential of UF_4^+ was measured also by Hildenbrand [45], Dyke at al. [30], and Lau and Hildenbrand [52], who measured values of 9.96 ± 0.10, 10.32 and 10.2 ± 0.3 eV, respectively. The ionization potential of smaller ions from UF_4 neutral precursor was reported only by Lau and Hildenbrand [52], who measured 13.33 ± 0.10, 19.5 ± 0.5 and 25.5 ± 0.5 eV for UF_3^+, UF_2^+ and UF^+, respectively. All these values are in very good agreement with our measurements.

3.3. Vapour pressure of LiF-ThF_4-UF_4 (77.5-20.0-2.5 mol%)

Partial vapour pressure results obtained by KEMS for the mixture LiF-ThF_4-UF_4 (77.5-20.0-2.5 mol%) are listed in Annex Table 2. These results are well approximated by the equations in Table 5, which are displayed in Fig. 6.

Errors for slopes and intercepts in Table 5 refer to the uncertainty estimated considering possible deviations from reference values of temperature and cross sections. In this regard, ionization cross sections of the lithium species (monomer, dimer and trimer) were taken from Yamawaki et al. [27], who based their values on the work performed by Stafford [53]. Similarly to what has been mentioned in Section 3.2 for UF_4, we applied a relative uncertainty of ±20% also on the cross sections of lithium species and ThF_4, coming to similar conclusions. So, we suggest a confidence interval

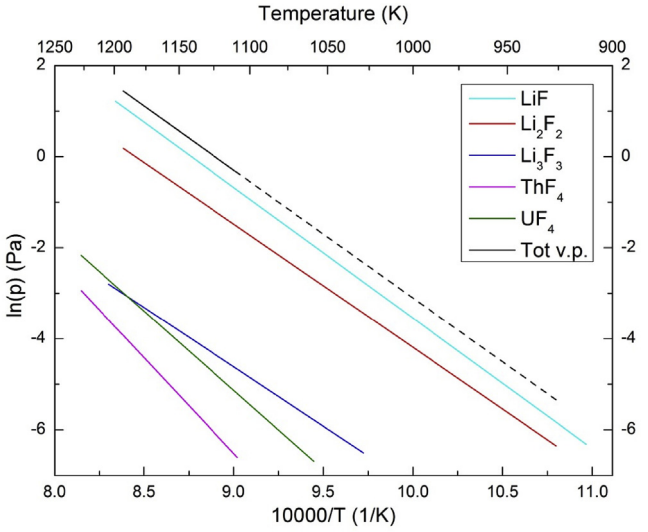

Fig. 6. Partial and total vapour pressures for the mixture LiF-ThF_4-UF_4 (77.5-20.0-2.5 mol%). The dashed line is the total vapour pressure considering only LiF and Li_2F_2 (their partial vapour pressures are several orders of magnitude higher than other species). Relative uncertainty on vapour pressure measurements is 50%.

±50% also on the results listed in Annex Table 2.

Lithium fluoride monomer and dimer are the species with the highest vapour pressure and the sum of their partial vapour pressures almost equals the total vapour pressure of the mixture in the temperature range considered. This does not surprise since LiF is the solvent of the mixture with a molar content of 77.5 mol%. The partial vapour pressure of UF_4 is higher than the one of ThF_4 despite a molar content of ThF_4 eight times higher than UF_4. Although it was not possible measuring the partial vapour pressure of all the species in the entire temperature range of operation of the MSFR (which may be between 923 and 1073 K [8]), since the temperature range of the measurement is very similar, the formulas listed in Table 5 can reasonably be extrapolated to this range.

The departure from ideal behaviour was quantified using Raoult's law, which states that the partial vapour pressure of each component (p_i^{ideal}) of an ideal mixture of liquids is equal to the vapour pressure of the pure component (p_i^*) normalized (multiplied) by its mole fraction in the mixture (x_i):

$$p_i^{ideal} = p_i^* x_i \tag{11}$$

Because the reference state is liquid, the vapour pressures of the pure components in equation (11) are taken from formulas for the vapour pressure in the liquid extrapolated to the supercooled state. The used formulas are listed in Table 6.

For lithium fluoride species and ThF_4 we used the equations of

Table 5
Formulas for partial and total vapour pressures for the mixture LiF-ThF_4-UF_4 (77.5-20.0-2.5) based on the values measured in this work.

Species	Equation	Temp range [K]
LiF(g)	$\ln p(Pa) = -\frac{(28678 \pm 284)}{T(K)} + (25.134 \pm 0.204)$	912–1198
Li_2F_2(g)	$\ln p(Pa) = -\frac{(27071 \pm 268)}{T(K)} + (22.883 \pm 0.208)$	926–1193
Li_3F_3(g)	$\ln p(Pa) = -\frac{(26052 \pm 261)}{T(K)} + (18.830 \pm 0.213)$	1028–1204
Tot LiF species	$\ln p(Pa) = -\frac{(28151 \pm 271)}{T(K)} + (25.043 \pm 0.199)$	1028–1193
ThF_4(g)	$\ln p(Pa) = -\frac{(41987 \pm 420)}{T(K)} + (31.273 \pm 0.213)$	1109–1227
UF_4(g)	$\ln p(Pa) = -\frac{(34804 \pm 348)}{T(K)} + (26.190 \pm 0.213)$	1059–1227
Tot vap pressure	$\ln p(Pa) = -\frac{(28277 \pm 276)}{T(K)} + (25.166 \pm 0.203)$	1109–1193

Table 6
Vapour pressure formulas of pure components used in this work. Errors for slopes and intercepts correspond to the values provided by the authors [11,46].

Species	Equation	Ref
LiF(g)	$\ln p(Pa) = -\frac{(28064\pm159)}{T(K)} + (25.893\pm0.124)$	[11]
Li_2F_2(g)	$\ln p(Pa) = -\frac{(27707\pm69)}{T(K)} + (24.886\pm0.055)$	[11]
Li_3F_3(g)	$\ln p(Pa) = -\frac{(24566\pm203)}{T(K)} + (19.305\pm0.161)$	[11]
ThF_4(g)	$\ln p(Pa) = -\frac{(34858\pm180)}{T(K)} + (29.386\pm0.124)$	[11]
UF_4(g)	$\ln p(Pa) = -\frac{(27663\pm771)}{T(K)} + (27.608\pm0.737)$	[46]

our previous work [11]. Because we could not measure UF_4 vapour pressure in the liquid state, we used the formula proposed by Nagarajan et al. [46] (adjusted for natural logarithm and pascal unit of pressure), who obtained results for the solid state in good agreement with ours. Fig. 7 compares the partial vapour pressures of the ideal mixture (dashed lines) and the ones based on the experimental values (solid lines). Results obtained by thermodynamic calculations based on the database assessed by Capelli et al. [39] are also shown in Fig. 7 (dotted lines).

In the considered range (≈900–1250 K), the calculations overestimate the total vapour pressure lithium fluoride species of a factor 1.5 and partial vapour pressure of ThF_4 and UF_4 of a factor 7.9 and 3.6 on average, respectively. These large values might be explained because no ternary parameter was used for the system LiF-ThF_4-UF_4 since the excess Gibbs energies were calculated purely based on the corresponding binary sub-systems. For LiF-ThF_4 data on phase equilibria, enthalpy of mixing and enthalpy of the eutectic composition were used, but for ThF_4-UF_4 and LiF-UF_4 only equilibrium phase diagram data were used. This may explain the discrepancies between the measurement and the calculation.

The ideal behaviour overestimates the vapour pressure of lithium fluoride species of a factor 3. On the ln(p) vs 1/T diagram, the partial vapour pressures of ThF_4 and UF_4 show different slopes from the experimental observation, leading to very much higher values (up to hundreds of times), especially at lower temperatures (900–1000 K). This is not reproduced by the calculations, which give slopes more consistent with the experimental observation.

In Table 7, the activity coefficients of the end-members of the mixture LiF-ThF_4-UF_4 (77.5-20.0-2.5 mol%), in the range

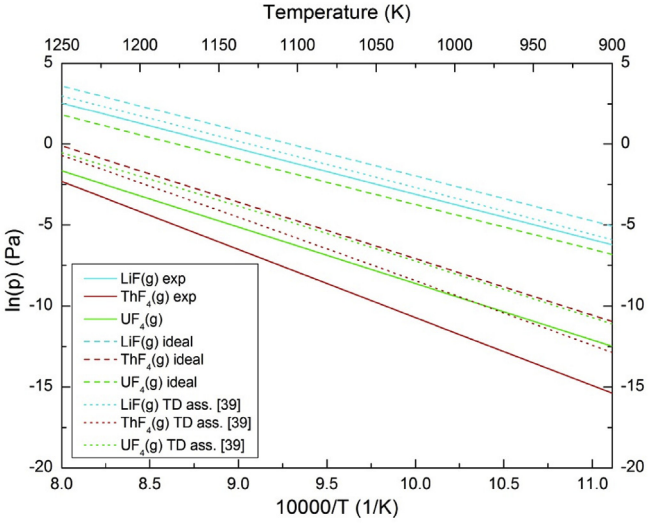

Fig. 7. Comparison of partial vapour pressures of the mixture LiF-ThF_4-UF_4 (77.5-20.0-2.5 mol%) with ideal behaviour and thermodynamic (TD) assessment based on [39].

Table 7
Activity coefficients for the mixture LiF-ThF_4-UF_4 (77.5-20.0-2.5 mol%).

Species	900 K	1000 K	1100 K	1200 K	1300 K
LiF	0.315	0.323	0.331	0.338	0.345
ThF_4	0.012	0.026	0.051	0.087	0.137
UF_4	0.003	0.008	0.015	0.025	0.040

900–1300 K are determined according to the relation:

$$\gamma_i = \frac{p_i^{exp}}{x_i p_i^*} \tag{12}$$

where p_i^{exp} and p_i^* are the experimental partial vapour pressure of the species i in the mixture and the vapour pressure of the pure component i, respectively. Their values are determined using the equations listed in Tables 5 and 6 These values quantify the departure from the ideal behaviour discussed in the previous paragraphs.

Finally, the boiling point of the mixture LiF-ThF_4-UF_4 (77.5-20.0-2.5 mol%) was extrapolated from the measured total vapour pressure (sum of all the partial vapour pressures) to 1 bar pressure. Based on this approach, we recommend for the mixture LiF-ThF_4-UF_4 (77.5-20.0-2.5 mol%) a boiling point of 2019 ± 10 K, which is just 2 K lower than the predicted value based on the thermodynamic assessment [39]. It is important to consider that at high temperatures, the composition of the mixture differs from the initial one. According to our calculations (based on the Hertz-Knudsen equation [22]), LiF, UF_4 and ThF_4 lost 1% of their initial masses during the KEMS experiment approximately at 1135, 1180 and 1290 K, respectively, from which we can conclude that below 1135 K the composition of the melt remained unchanged within ±1 mol% uncertainty. These phenomena should be taken into account for the boiling point measurement of the MSFR fuel mixture.

4. Conclusions

In this work, experimental results for the vaporization behaviour of a selected mixture for the MSFR are presented and discussed. Thorium and uranium tetrafluoride were synthetized and the mixture LiF-ThF_4-UF_4 (77.5-20.0-2.5 mol%) was prepared and analysed by KEMS.

Experimental results and equations for partial and total vapour pressures of this mixture are provided. The results on the vapour pressure of the pure end-members, performed in this (UF_4) and our previous study (LiF and ThF_4) [11], are in good agreement with literature data increasing the reliability of partial vapour pressure results for the mixture LiF-ThF_4-UF_4 (77.5-20.0-2.5 mol%). Since data were collected within temperature ranges very similar to the operating temperature of the MSFR, the proposed formulas are reasonably reliable also for that range.

Experimental results for the mixture LiF-ThF_4-UF_4 (77.5-20.0-2.5 mol%) were used to calculate the activity coefficients, quantifying the departure from ideal behaviour at different temperatures. Raoult's law was used for calculating partial vapour pressures in the ideal case, giving values 3 times higher than the experimental ones for LiF. In the ideal case, on the ln(p) vs 1/T diagram, ThF_4 and UF_4 show a rather different slope if compared with the experimental results. This change of slope was not observed in the calculations using the thermodynamic database assessed by Capelli et al. [39]. However, also the calculations overestimate the experimental values significantly. This may be due to the lack of ternary parameters for the system LiF-ThF_4-UF_4, and of vapour pressure data in the model, giving suggestions for future works.

Novel results on the vapour pressure of solid uranium

tetrafluoride are presented finding a good agreement with several available literature data. Second and third law treatment of the experimental data gave values for the enthalpy of sublimation of 314.0 ± 0.8 kJ/mol and 314.0 ± 0.4 kJ/mol, respectively. These results are in very good agreement with the values obtained by a third law treatment of experimental data in several independent studies. The appearance potential of neutral UF_4 precursor was measured for several ionization reactions. The results for UF_4^+, UF_3^+, UF_2^+ and UF^+ are in good agreement with available literature data, while no result for U^+ was found in literature for comparison.

The melting point of the mixture LiF-ThF_4-UF_4 (77.5-20.0-2.5 mol%) was experimentally assessed by DSC as 828 ± 3 K. The pseudo binary phase for the LiF-ThF_4 system with 2.5 mol% of UF_4 (calculated using the database of our previous thermodynamic assessment [39]) indicates an eutectic temperature which is in very good agreement with the experimental value. The boiling point of the mixture LiF-ThF_4-UF_4 (77.5-20.0-2.5 mol%) was assessed extrapolating experimental data by KEMS to the atmospheric pressure, giving a value of 2019 ± 10 K. The boiling point determined using the thermodynamic database assessed by Capelli et al. [39] (2021 K) is in very good agreement with this value.

Acknowledgements

The authors would like to thank Konstantinos Bobordis for valuable discussion on measurement uncertainty. This work was partially funded by the Euratom research and training programme 2014–2018 under grant agreement No 661891 (SAMOFAR).

Annex tables

Annex Table 1
Vapour pressure results of UF_4 obtained by KEMS in this work.

Temp [K]	p [Pa]	Temp [K]	p [Pa]	Temp [K]	p [Pa]	Temp [K]	p [Pa]
1081.4	1.64E+00	1119.1	4.64E+00	1153.6	1.16E+01	1186.3	2.88E+01
1082.9	1.72E+00	1120.8	4.86E+00	1154.9	1.20E+01	1186.8	2.90E+01
1084.7	1.80E+00	1122.7	5.08E+00	1155.9	1.24E+01	1187.0	2.92E+01
1086.4	1.89E+00	1124.6	5.32E+00	1157.2	1.28E+01	1187.2	2.95E+01
1088.0	1.97E+00	1126.2	5.57E+00	1158.2	1.32E+01	1187.6	2.96E+01
1090.0	2.07E+00	1127.9	5.84E+00	1159.7	1.36E+01	1187.6	2.97E+01
1091.6	2.17E+00	1129.8	6.09E+00	1160.7	1.40E+01	1187.7	2.99E+01
1093.2	2.28E+00	1131.3	6.36E+00	1161.8	1.44E+01	1187.9	3.00E+01
1094.7	2.38E+00	1132.6	6.62E+00	1163.1	1.49E+01	1187.9	3.00E+01
1096.7	2.49E+00	1134.1	6.93E+00	1164.4	1.56E+01	1187.7	3.00E+01
1098.6	2.61E+00	1135.8	7.22E+00	1165.7	1.60E+01	1187.9	3.01E+01
1100.0	2.74E+00	1137.1	7.50E+00	1167.1	1.65E+01	1189.3	3.29E+01
1101.8	2.86E+00	1138.8	7.80E+00	1172.6	2.04E+01	1190.1	3.36E+01
1103.2	2.98E+00	1140.0	8.09E+00	1174.2	2.11E+01	1191.0	3.42E+01
1104.8	3.13E+00	1141.4	8.40E+00	1175.7	2.18E+01	1192.2	3.50E+01
1106.5	3.26E+00	1142.9	8.67E+00	1177.0	2.26E+01	1193.1	3.58E+01
1107.8	3.40E+00	1143.3	8.85E+00	1178.2	2.33E+01	1194.1	3.66E+01
1109.2	3.53E+00	1144.2	9.07E+00	1179.4	2.40E+01	1195.4	3.75E+01
1110.6	3.65E+00	1145.0	9.29E+00	1180.5	2.48E+01	1196.5	3.84E+01
1111.8	3.79E+00	1146.3	9.56E+00	1181.7	2.55E+01	1197.1	3.93E+01
1113.3	3.89E+00	1147.3	9.84E+00	1182.7	2.62E+01	1198.3	4.03E+01
1114.2	4.03E+00	1148.5	1.02E+01	1183.7	2.68E+01	1199.4	4.13E+01
1115.4	4.16E+00	1149.8	1.05E+01	1184.5	2.74E+01	1200.4	4.23E+01
1116.4	4.32E+00	1151.3	1.09E+01	1185.3	2.79E+01		
1118.0	4.46E+00	1152.4	1.12E+01	1185.9	2.84E+01		

Annex Table 2
Partial vapour pressure results for the mixture LiF-ThF_4-UF_4 (77.5-20.0-2.5 mol%).

LiF		**Li_2F_2**		**Li_3F_3**		**ThF_4**		**UF_4**	
Temp [K]	P (LiF)	Temp [K]	P (Li_2F_2)	Temp [K]	P (Li_3F_3)	Temp [K]	P (ThF_4)	Temp [K]	P (ThF_4)
912.0	1.64E-03	926.1	1.77E-03	1028.4	1.55E-03	1108.6	1.38E-03	1058.6	1.20E-03
920.5	2.43E-03	933.3	2.17E-03	1035.7	1.78E-03	1115.0	1.69E-03	1065.2	1.53E-03
928.0	2.81E-03	940.3	2.72E-03	1042.7	2.09E-03	1122.5	2.26E-03	1071.5	2.03E-03
935.2	4.08E-03	948.1	3.39E-03	1049.2	2.45E-03	1130.3	2.86E-03	1078.5	2.29E-03
942.7	4.92E-03	955.5	4.05E-03	1056.1	2.89E-03	1137.3	3.67E-03	1084.9	3.00E-03
950.1	6.29E-03	962.3	4.89E-03	1062.4	3.37E-03	1143.6	4.48E-03	1091.2	3.52E-03
957.4	7.65E-03	968.9	6.01E-03	1069.2	3.89E-03	1150.1	5.50E-03	1097.1	4.07E-03
964.1	9.10E-03	975.8	7.19E-03	1075.8	4.56E-03	1156.2	6.20E-03	1102.8	4.63E-03
970.7	1.32E-02	982.6	8.82E-03	1082.3	5.23E-03	1162.1	7.83E-03	1108.7	5.63E-03
977.7	1.64E-02	989.8	1.16E-02	1088.8	6.03E-03	1164.6	8.14E-03	1115.2	6.39E-03
984.6	2.01E-02	996.9	1.44E-02	1094.6	6.72E-03	1165.5	8.10E-03	1122.8	8.09E-03
991.6	2.40E-02	1003.3	1.70E-02	1100.4	7.61E-03	1168.2	9.11E-03	1130.5	9.56E-03
998.9	2.96E-02	1009.7	2.03E-02	1106.5	8.38E-03	1172.0	1.02E-02	1137.6	1.18E-02
1005.0	3.53E-02	1018.5	2.45E-02	1112.3	1.06E-02	1176.8	1.18E-02	1143.8	1.39E-02
1012.2	4.23E-02	1026.6	3.11E-02	1119.1	1.21E-02	1181.7	1.37E-02	1150.3	1.64E-02

Annex Table 2 (*continued*)

LiF		Li_2F_2		Li_3F_3		ThF_4		UF_4	
Temp [K]	P (LiF)	Temp [K]	P (Li_2F_2)	Temp [K]	P (Li_3F_3)	Temp [K]	P (ThF_4)	Temp [K]	P (ThF_4)
1020.8	5.07E-02	1034.2	3.87E-02	1127.6	1.40E-02	1186.4	1.63E-02	1156.4	1.87E-02
1028.5	6.49E-02	1041.1	4.52E-02	1134.6	1.64E-02	1191.1	1.84E-02	1162.3	2.18E-02
1036.1	7.93E-02	1047.9	5.37E-02	1141.2	1.90E-02	1195.4	2.07E-02	1164.5	2.35E-02
1043.0	9.64E-02	1054.4	6.25E-02	1147.6	2.17E-02	1200.9	2.49E-02	1165.5	2.49E-02
1049.6	1.12E-01	1060.9	7.55E-02	1153.6	2.45E-02	1206.7	2.93E-02	1168.3	2.65E-02
1056.4	1.34E-01	1067.6	8.83E-02	1159.7	2.75E-02	1212.4	3.59E-02	1172.2	2.96E-02
1062.9	1.62E-01	1074.1	1.03E-01	1165.0	3.04E-02	1217.1	4.13E-02	1176.7	3.36E-02
1069.2	1.89E-01	1080.9	1.20E-01	1164.8	3.06E-02	1221.3	4.62E-02	1181.8	3.77E-02
1076.1	2.21E-01	1087.3	1.39E-01	1166.8	3.16E-02	1227.1	5.54E-02	1186.5	4.32E-02
1082.9	2.60E-01	1093.3	1.60E-01	1170.2	3.32E-02			1191.2	4.90E-02
1089.1	3.04E-01	1099.0	1.83E-01	1174.8	3.53E-02			1195.4	5.50E-02
1095.1	3.48E-01	1105.1	2.09E-01	1179.5	3.83E-02			1201.1	6.33E-02
1100.7	4.01E-01	1111.2	2.38E-01	1184.7	4.16E-02			1206.7	7.29E-02
1106.9	4.60E-01	1117.6	2.71E-01	1189.3	4.48E-02			1212.5	8.30E-02
1112.7	5.28E-01	1125.9	3.18E-01	1193.6	4.83E-02			1217.2	9.32E-02
1119.5	6.10E-01	1133.0	3.71E-01	1198.7	5.14E-02			1221.5	1.06E-01
1127.8	7.13E-01	1139.8	4.24E-01	1204.4	5.65E-02			1227.2	1.22E-01
1134.8	8.39E-01	1146.1	4.83E-01						
1141.4	9.61E-01	1152.4	5.38E-01						
1147.7	1.09E+00	1158.4	6.20E-01						
1153.9	1.21E+00	1164.3	6.88E-01						
1160.0	1.50E+00	1164.8	7.02E-01						
1165.0	1.69E+00	1166.2	7.19E-01						
1164.9	1.76E+00	1169.6	7.56E-01						
1167.0	1.82E+00	1173.6	8.04E-01						
1170.4	1.94E+00	1178.5	8.69E-01						
1175.1	2.10E+00	1183.5	9.38E-01						
1179.8	2.29E+00	1188.1	1.01E+00						
1184.9	2.51E+00	1192.7	1.07E+00						
1189.4	2.76E+00								
1193.9	3.01E+00								
1198.8	3.26E+00								

References

[1] J. Serp, M. Allibert, O. Beneš, S. Delpech, O. Feynberg, V. Ghetta, D. Heuer, D. Holcomb, V. Ignatiev, J.L. Kloosterman, L. Luzzi, E. Merle-Lucotte, J. Uhlíř, R. Yoshioka, D. Zhimin, The molten salt reactor (MSR) in generation IV: overview and perspectives, Prog. Nucl. Energy 77 (2014) 308–319, https://doi.org/10.1016/j.pnucene.2014.02.014.

[2] US DOE Nuclear Energy Research Advisory Committee and the Generation IV In-ternational Forum, a Technology Roadmap for Generation IV Nuclear Energy Systems, 2002, https://doi.org/10.2172/859029.

[3] T.J. Dolan, Molten Salt Reactors and Thorium Energy, Woodhead Publishing, 2017.

[4] L. Mathieu, D. Heuer, E. Merle-Lucotte, R. Brissot, C. Le Brun, E. Liatard, J.-M. Loiseaux, O. Méplan, A. Nuttin, D. Lecarpentier, Possible configurations for the thorium molten salt reactor and advantages of the fast nonmoderated version, Nucl. Sci. Eng. 161 (2009) 78–89, https://doi.org/10.13182/NSE07-49.

[5] M. Allibert, M. Aufiero, M. Brovchenko, S. Delpech, V. Ghetta, D. Heuer, A. Laureau, E. Merle-Lucotte, Molten Salt Fast Reactors, 2016, https://doi.org/10.1016/B978-0-08-100149-3.00007-0.

[6] OECD Nuclear Energy Agency, Technology Roadmap Update for Generation IV Nuclear Energy Systems, 2014, pp. 1–66. https://www.gen-4.org/gif/upload/docs/application/pdf/2014-03/gif-tru2014.pdf.

[7] K. van der Graaf, J.L. Kloosterman, A Paradigm Shift in Nuclear Reactor Safety with the Molten Salt Fast Reactor, November, 23, 2015. www.samofar.eu.

[8] M. Allibert, D. Gérardin, D. Heuer, E. Huffer, A. Laureau, E. Merle, S. Beils, A. Cammi, B. Carluec, S. Delpech, A. Gerber, E. Girardi, J. Krepel, D. Lathouwers, D. Lecarpentier, S. Lorenzi, L. Luzzi, M. Ricotti, V. Tiberi, SAMOFAR European Project D1.1 Description of Initial Reference Design and Identification of Safety Aspects, 2017. Contract number: 661891.

[9] D. Heuer, E. Merle-Lucotte, M. Allibert, M. Brovchenko, V. Ghetta, P. Rubiolo, Towards the thorium fuel cycle with molten salt fast reactors, Ann. Nucl. Energy 64 (2014) 421–429, https://doi.org/10.1016/j.anucene.2013.08.002.

[10] E. Merle-Lucotte, D. Heuer, M. Allibert, M. Brovchenko, N. Capellan, V. Ghetta, Launching the Thorium Fuel Cycle with the Molten Salt Fast Reactor, International Congress on Advances in Nuclear Power Plants (ICAPP 2011), Nice, France, 2011, pp. 842–851.

[11] E. Capelli, O. Beneš, J.-Y. Colle, R.J.M. Konings, Determination of the thermodynamic activities of LiF and ThF_4 in the $Li_x\ Th_{1-x}\ F_{4-3x}$ liquid solution by Knudsen effusion mass spectrometry, Phys. Chem. Chem. Phys. 17 (2015) 30110–30118, https://doi.org/10.1039/C5CP04777C.

[12] P. Souček, O. Beneš, B. Claux, E. Capelli, M. Ougier, V. Tyrpekl, J.-F. Vigier, R.J.M. Konings, Synthesis of UF_4 and ThF_4 by HF gas fluorination and re-determination of the UF_4 melting point, J. Fluorine Chem. 200 (2017) 33–40, https://doi.org/10.1016/j.jfluchem.2017.05.011.

[13] R.B. Briggs, Molten-salt Reactor Program Semiannual Progress Report for Period Ending July 31, 1964. ORNL-3708, 1964, http://technicalreports.ornl.gov/1964/3445600500358.pdf.

[14] O. Beneš, R.J.M. Konings, S. Wurzer, M. Sierig, A. Dockendorf, A DSC study of the $NaNO_3$-KNO_3 system using an innovative encapsulation technique, Thermochim. Acta 509 (2010) 62–66, https://doi.org/10.1016/j.tca.2010.06.003.

[15] K. Hilpert, High-temperature mass spectrometry in materials research, Rapid Commun. Mass Spectrom. 5 (1991) 175–187, https://doi.org/10.1002/rcm.1290050408.

[16] J. Drowart, C. Chatillon, J. Hastie, D. Bonnell, High-temperature mass spectrometry: instrumental techniques, ionization cross-sections, pressure measurements, and thermodynamic data (IUPAC Technical Report), Pure Appl. Chem. 77 (2005) 683–737, https://doi.org/10.1351/pac200577040683.

[17] J.P. Hiernaut, J.Y. Colle, R. Pflieger-Cuvellier, J. Jonnet, J. Somers, C. Ronchi, A Knudsen cell-mass spectrometer facility to investigate oxidation and vaporisation processes in nuclear fuel, J. Nucl. Mater. 344 (2005) 246–253, https://doi.org/10.1016/j.jnucmat.2005.04.050.

[18] J.-Y. Colle, D. Freis, O. Bene, R.J.M. Konings, Knudsen effusion mass spectrometry of nuclear materials: applications and developments, ECS Trans. 46 (2013) 23–38, https://doi.org/10.1149/04601.0023ecst.

[19] F. Capone, J.-Y. Colle, J.P. Hiernaut, C. Ronchi, Mass spectrometric measurement of the ionization energies and cross sections of uranium and plutonium oxide vapors, J. Phys. Chem. A 103 (1999) 10899–10906, https://doi.org/10.1021/jp992405f.

[20] R. Hultgren, R. Orr, P. Anderson, K. Kelley, Selected Value of Thermodynamic Properties of Metals and Alloys, John Wiley and Sons, Inc, 1963.

[21] R.G. Livesey, Flow of gases through tubes and orifices, Found. Vac. Sci. Technol (1998) 25, https://doi.org/10.1063/1.882616.

[22] R. Grimley, The Characterization of High Temperature Vapours, John Wiley and Sons, Inc, 1967.

[23] D.W. Bonnell, PROGRAM SIGMAS, Ver 1.11 NIST, USA vol. 301, 1990, pp. 975–5755 (n.d.).

[24] J.B. Mann, Ionization cross sections of the elements calculated from mean-square radii of atomic orbitals, J. Chem. Phys. 46 (1967) 1646, https://doi.org/10.1063/1.1840917.

[25] H. Deutsch, K. Becker, T.D. Märk, A modified additivity rule for the calculation of electron impact ionization cross-section of molecules ABn, Int. J. Mass Spectrom. Ion Process 167–168 (1997) 503–517, https://doi.org/10.1016/

S0168-1176(97)00108-0.
[26] J.P. Desclaux, Relativistic Dirac-Fock expectation values for atomos with Z=1 to Z=120, At. Data Nucl. Data Tables 12 (1973) 311–406.
[27] M. Yamawaki, M. Hirai, M. Yasumoto, M. Kanno, Mass spectrometric study of vaporization of lithium fluoride, J. Nucl. Sci. Technol. 19 (1982) 563–570.
[28] R. Grimley, J. Forsman, Q. Grindstaff, A mass spectrometric study of the fragmentation of the lithium fluoride vapor system, J. Phys. Chem. 82 (1978) 632–638.
[29] R.F. Porter, R.C. Schoonmaker, Mass spectrometric study of the vaporization of LiF, NaF, and LiF–NaF mixtures, J. Chem. Phys. 29 (1958) 1070–1074, https://doi.org/10.1063/1.1744657.
[30] J.M. Dyke, N.K. Fayad, A. Morris, I.R. Trickle, G.C. Allen, A study of the electronic structure of the actinide tetrahalides UF_4, ThF_4, UCl_4 and $ThCl_4$ using vacuum ultraviolet photoelectron spectroscopy and SCF-Xα scattered wave calculations, J. Chem. Phys. 72 (1980) 3822, https://doi.org/10.1063/1.439597.
[31] R.J.M. Konings, J.P.M. Van Der Meer, E. Walle, Chemical Aspects of Molten Salt Reactor Fuel and Coolant - Cordis, (n.d.) 1–76.
[32] M.W. Chase Jr., NIST-JANAF thermochemical tables fourth edition, J. Phys. Chem. Ref. Data 9 (1998).
[33] E.P. Dergunov, A.G. Bergman, Complex formation between alkali metal fluorides and fluorides of metals of the fourth group, Dokl. Akad. Nauk SSSR 60 (1948) 391–394.
[34] W.J. Asker, E.R. Segnit, A.W. Wylie, 857. The potassium thorium fluorides, J. Chem. Soc. (1952) 4470, https://doi.org/10.1039/jr9520004470.
[35] R.E. Thoma, H. Insley, B.S. Landau, H.A. Friedman, W.R. Grimes, Phase equilibria in the fused salt systems LiF–ThF_4 and NaF–ThF_4, J. Phys. Chem. 63 (1959) 1266–1274, https://doi.org/10.1021/j150578a013.
[36] A.S. Dworkin, M.A. Bredig, Enthalpy of lanthanide chlorides, bromides, and iodides from 298-1300 K: Enthalpy of fusion and transition, High Temp. Sci. 3 (1971) 81–90.
[37] L.A. Khripin, Y.V. Gagarinskii, L.A. Luk'yanova, Phase transitions of uranium tetrafluoride and tetrachloride, Izv. Sib. Otd. Akad. Nauk SSSR, No. 3, Ser. Khim. Nauk 1 (1965) 14–19.
[38] M.M. Popov, F.A. Kostylev, N.V. Zubova, Vapour pressure of uranium tetrafluoride, Russ. J. Inorg. Chem. 4 (1959) 770–771.
[39] E. Capelli, O. Beneš, R.J.M. Konings, Thermodynamic assessment of the LiF-ThF_4-PuF_3-UF_4 system, J. Nucl. Mater. 462 (2015) 43–53, https://doi.org/10.1016/j.jnucmat.2015.03.042.
[40] A.D. Pelton, P. Chartrand, G. Eriksson, The modified quasi-chemical model: Part IV. Two-sublattice quadruplet approximation, Metall. Mater. Trans. A Phys. Metall. Mater. Sci. 32 (2001) 1409–1416, https://doi.org/10.1007/s11661-001-0230-7.
[41] A.D. Ryon, L.P. Twichell, Vapor Pressure and Related Physical Constants of Uranium Tetrafluoride, 1947. H-5.385.2.
[42] S. Langer, F.F. Blankenship, The vapour pressure of uranium tetrafluoride, J. Inorg. Nucl. Chem. 14 (1960) 26–31, https://doi.org/10.1016/0022-1902(60)80194-7.
[43] P.A. Akishin, Y.S. Khodeev, Determination of the heat of sublimation of uranium tetrafluoride by the mass-spectroscopic method, Russ. J. Phys. Chem. 35 (1961) 574–575.
[44] E.G. Chudinov, D.Y. Choporov, Saturated vapor pressure of solid uranium tetrafluoride, Russ. J. Phys. Chem. 44 (1970) 1106–1109.
[45] D.L. Hildenbrand, Thermochemistry of gaseous uranium pentafluoride and uranium tetrafluoride, J. Chem. Phys. 66 (1977) 4788–4794, https://doi.org/10.1063/1.433841.
[46] K. Nagarajan, M. Bhupathy, R. Prasad, Z. Singh, V. Venugopal, D.D. Sood, Vaporization behaviour of uranium tetrafluoride, J. Chem. Thermodyn. 12 (1980) 329–333, https://doi.org/10.1016/0021-9614(80)90144-5.
[47] K.O. Johnsson, The Vapor Pressure of Uranium Tetrafluoride, Report Y-42, Clinton Engineer Works, Carbon and Carbon Chemicals Corporation, 1947. Y-12 Plant, Oak Ridge, Tennessee, USA.
[48] I. Grenthe, J. Fuger, R.J.M. Konings, R.J. Lemire, A.B. Muller, C. Nguyen-Trung Cregu, H. Wanner, Chemical thermodynamics of uranium, 2004, https://doi.org/10.1063/1.473182.
[49] R. Guillamont, T. Fanghänel, V. Neck, F. Jean, D.A. Palmer, I. Grenthe, M.H. Rand, Update on the Chemical Thermodynamics of Uranium, Neptunium, Plutonium, Americium and Technetium, Amsterdam, 2003.
[50] G.N. Lewis, M. Randall, , K.S. revised by Pitzer, L. Brewer, Thermodynamics, third ed., McGrew-Hill, 1995.
[51] L.N. Gorokhov, V.K. Smirnov, Y.S. Khodeev, Thermochemical characteristics of uranium fluoride UFn molecules, Russ. J. Phys. Chem. 58 (1984) 980–983.
[52] K.H. Lau, D.L. Hildenbrand, Thermochemical properties of the gaseous lower valent fluorides of uranium, J. Chem. Phys. 76 (1982) 2646–2652, https://doi.org/10.1063/1.443246.
[53] F.E. Stafford, Calculation of electron impact ionization cross sections, in: Mass Spectrom. Inorg. Chem. Adv. Chem., 1968, pp. 115–126, https://doi.org/10.1021/ba-1968-0072.ch009.